

Adaptive Visual Autoregressive Acceleration via Dual-Linkage Entropy Analysis

Yu Zhang¹ Jingyi Liu¹ Feng Liu² Duoqian Miao¹ Qi Zhang¹ Kexue Fu³ Changwei Wang³ Longbing Cao⁴



Figure 1. NOVA generates a 2K image in 3.2 seconds on a single NVIDIA RTX 3090 GPU without running out of GPU memory.

Abstract

Visual AutoRegressive modeling (VAR) suffers from substantial computational cost due to the massive token count involved. Failing to account for the continuous evolution of modeling dynamics, existing VAR token reduction methods face three key limitations: heuristic stage partition, non-adaptive schedules, and limited acceleration scope, thereby leaving significant acceleration potential untapped. Since entropy variation intrinsically reflects the transition of predictive uncertainty, it offers a principled measure to capture modeling dynamics evolution. Therefore, we propose NOVA, a training-free token reduction acceleration framework for VAR models via entropy analysis. NOVA adaptively determines the acceleration activation scale during inference by online identifying the inflection point of scale entropy growth. Through scale-linkage and layer-linkage ratio adjustment, NOVA dynamically computes distinct token reduction ratios for each scale and layer, pruning low-entropy tokens while reusing the cache derived from the residuals at the prior

scale to accelerate inference and maintain generation quality. Extensive experiments and analyses validate NOVA as a simple yet effective training-free acceleration framework.

1. Introduction

Recently, Visual AutoRegressive modeling (VAR) (Tian et al., 2024) based on next-scale prediction has demonstrated impressive breakthroughs in visual generation, achieving performance comparable to mainstream diffusion models (Shen et al., 2025; Croitoru et al., 2023; Cao et al., 2024). However, VAR’s performance improvement comes at the expense of a substantial computational cost. As illustrated in Figure 2, its inefficiency mainly stems from the considerable computation complexity caused by the excessive token count, which further hinders its scalability to higher-resolution visual generation and integration into other downstream tasks.

Towards direct and efficient application of VAR, training-free token reduction methods (Guo et al., 2025a; Chen et al., 2025b; Li et al., 2025d) have emerged as promising acceleration solutions. These methods build on a common observation: VAR’s substantial computational cost mainly occurs in the later stage. Consequently, they perform token reduction at this stage to accelerate inference. Although these methods achieve impressive results, they still face

¹Tongji University ²Harbin Institute of Technology ³Shandong Academy of Sciences ⁴Macquarie University. Correspondence to: Duoqian Miao <dqmiao@tongji.edu.cn>.

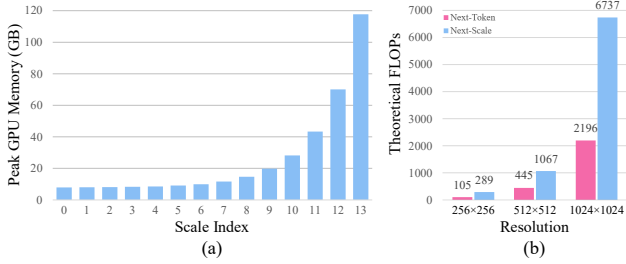


Figure 2. (a) Peak GPU memory consumption across different scales during 1024×1024 image generation in VAR. As the scale increases, the token sequence length grows rapidly, leading to quadratic growth in attention computation complexity. (b) Theoretical GFLOPs required by next-token and next-scale prediction models to generate images of various resolutions under uniform settings. Compared to the raster-scan next-token prediction, VAR’s coarse-to-fine next-scale prediction additionally requires predicting feature maps at multiple previous scales before generating the final scale. The cumulative computation at these previous transition scales introduces extra computational cost to VAR.

three key limitations: (1) *Heuristic stage partition*. The later stage partition heavily relies on statistical estimation or empirical observation. The precision of this boundary is critical: premature token reduction risks quality degradation, while delayed token reduction limits acceleration gains. (2) *Non-adaptive schedules*. All instances share the fixed stage boundary and token reduction ratio. However, different instance images vary enormously in complexity regarding semantics, composition, structure, lighting, and texture. The fixed stage partition and reduction ratio cannot guarantee optimality for every instance. (3) *Limited acceleration scope*. Token reduction is performed only in the partitioned later stage, leaving potential computational redundancy in earlier stages unaddressed.

We attribute above limitations to a fundamental oversight: treating scales and layers as isolated units while neglecting the continuous evolution of modeling dynamics across scales and layers. Specifically, these methods rigidly partition the later stage and independently optimize the token reduction objectives for each scale or layer in the later stage. However, VAR inherently follows a coarse-to-fine transitional process that necessitates consideration of continuous modeling evolution across both scales and layers. Thus, we argue that it is essential to adopt a dual-linkage (scales and layers) adaptive token reduction method.

From the viewpoint of information theory, autoregressive generation is essentially a process of progressively reducing sequential uncertainty through successive observations. Each token generation represents a new observation. As a direct measure of uncertainty, entropy effectively reflects the change in predictive uncertainty throughout the process. A high-entropy token signifies a highly uncertain prediction with the newly observed information that may significantly impact subsequent distribution predictions, typically corresponding to larger potential for entropy reduc-

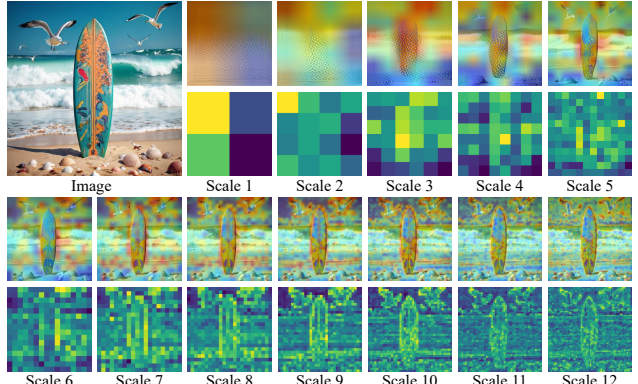


Figure 3. Entropy heatmaps of visualized images and token maps.

tion. Therefore, accurately modeling it offers substantial information gain¹ to further reduce sequential predictive uncertainty. Conversely, low-entropy tokens correspond to confident predictions for the current states with limited marginal impact on further narrowing distributions. Moreover, entropy variation allows us to analyze the uncertainty reduction process across scales or layers, thereby capturing the evolution of modeling dynamics. Meanwhile, as visualized in Figure 3, entropy heatmaps intuitively reveal the spatio-temporal diffusion characteristics of high-entropy regions: evolving from a globally concentrated pattern in early scales to a sparsely dispersed pattern in later scales. These analyses indicate that entropy naturally can serve as a principled token selection criterion for our dual-linkage adaptive token reduction method.

In light of the above discussion, we propose NOVA, a training-free acceleration framework for VAR models. Guided by entropy analysis, NOVA performs a dual-linkage adaptive token reduction across both scales and layers. Specifically, at the scale level, it adaptively determines the scale for acceleration activation by online identifying the inflection point in scale entropy growth curve, and computes a distinct token reduction ratio for each acceleration scale by a scale-linkage function. At the layer level, NOVA further utilizes a layer-linkage ratio adjustment function to determine the specific reduction ratio for each layer and reuses the cache from residual interpolation of the same layer at the prior scale to improve speed and maintain performance.

Extensive experiments and analysis demonstrate the effectiveness of NOVA. On GenEval, NOVA achieved a $2.89 \times$ speedup for Infinity-2B with only 0.01% performance loss, while surpassing comparable methods in both speed and performance. On ImageReward, NOVA not only reduced Infinity-8B’s latency from 1.51s to 0.75s, but even achieved a preference score surpassing the original Infinity-8B. We further provide extensive visualizations to demonstrate the NOVA’s excellent preservation of details and semantics.

¹Information gain, a fundamental concept in information theory, quantifies the reduction in predictive uncertainty.

2. Related Work

Next-Scale Visual AutoRegressive Generation. By converting raster-scan order prediction to next-scale prediction, Visual AutoRegressive modeling (VAR) (Tian et al., 2024) overcomes the limitations of next-pixel prediction and next-token prediction, which suffer from suboptimal performance due to disrupting the inherent spatial structure of images. Next-scale prediction and elevates generation quality to new heights. Some VAR-like variants, such as Infinity (Han et al., 2025), HART (Tang et al., 2024), STAR (Ma et al., 2024) and VAR-CLIP (Zhang et al., 2024) extend VAR to text-to-image generation. Other improved VAR-like models (Li et al., 2024b; Rajagopalan et al., 2025; Xie et al., 2024; Wu et al., 2025; Jiao et al., 2025; Qu et al., 2025; Wang et al., 2025) effectively perform various tasks.

Efficient Visual AutoRegressive Modeling. To address VAR’s efficiency bottleneck, numerous efforts (Huang et al., 2025; He et al., 2025; Kumar et al., 2025; Zhang et al., 2025b;a) have been made. However, all these methods necessitate major architectural modifications (Ren et al., 2024; Chen et al., 2025c; Vincenti et al., 2025) or extensive re-training (Tang et al., 2024; Kumbong et al., 2025), making them difficult to directly obtain and deploy. Training-free methods, such as FreqExit/SkipVAR’s early-exit inference or decision-based acceleration (Li et al., 2025b; Li et al.), ScaleKV/HACK’s KV-Cache optimization (Li et al., 2025c; Qin et al., 2025), and LiteVAR’s efficient attention and low-bit quantization (Xie et al., 2024), achieve good speedups but face some challenges, such as generation quality degradation due to coarse-grained execution units and suboptimal performance due to input-independent static acceleration. In contrast, training-free token reduction methods (Guo et al., 2025a; Chen et al., 2025b; Li et al., 2025d) have led the development of efficient VAR due to their strong generalizability and flexibility. However, due to the lack of adaptivity and dynamics, their acceleration potential remains unleashed.

Entropy-Guided Deep Learning. Entropy, as a measure of uncertainty and information distribution, is inherently linked to probabilistic modeling. Consequently, entropy-guided methods have been widely adopted in deep learning. Studies (Peer et al., 2022; Meni et al., 2024; Dubey et al., 2017) utilize entropy-based regularization to improve robustness and stability. SEGA (Wu et al., 2023a), MGEDE (Yang et al., 2023) and SEBot (Yang et al., 2024) enhance graph representation learning from an entropy perspective. EGGesture (Xiao et al., 2024) and EDRL (Wang et al., 2023) propose entropy-guided methods for VQ-VAE and disentangled representation learning, respectively. Meanwhile, entropy is also employed to improve efficiency, such as accelerating robotic visuomotor policies (Guo et al., 2025b), video diffusion models (Li et al., 2025a), and diffusion language

models (Ben-Hamu et al., 2025). However, its application to visual autoregressive generation almost leaves blanks.

3. Methodology

3.1. Preliminary

VAR (Tian et al., 2024) reformulates autoregressive modeling from next-token prediction to next-scale residual feature prediction, generating images in a coarse-to-fine manner. Formally, the modeling process involves T multi-scale token maps $\{R_1, R_2, \dots, R_T\} = \{R_t\}_{t=1}^T$, where $R_t \in [V]^{h_t \times w_t}$ and (h_t, w_t) denotes the grid size at scale t . At the t -th scale, VAR predicts the token map R_t conditioned on all previous scales $R_{<t} = \{R_1, R_2, \dots, R_{t-1}\}$. The autoregressive likelihood is formulated as follow:

$$p(R_1, R_2, \dots, R_T) = \prod_{t=1}^T p(R_t | \langle \text{sos} \rangle, R_{<t}), \quad (1)$$

where $\langle \text{sos} \rangle$ denotes the start conditional embedding.

3.2. Analysis

Theoretical Foundation for Entropy-Guided Token Reduction. In information theory, given a conditioning variable Z , the conditional mutual information between random variables X and Y satisfies

$$I(X; Y | Z) \leq H(X | Z), \quad (2)$$

where $H(X | Z)$ denotes the conditional entropy of X given Z , and conditional mutual information $I(X; Y | Z) = H(Y | Z) - H(Y | X, Z)$ measures information gain, i.e., the reduction in uncertainty of Y after observing X given Z .

VAR treats scales as autoregressive steps. For t -th scale, let $N_t = h_t w_t$ and denote the token at R_t spatial index $i \in \{1, \dots, N_t\}$ as $r_{t,i} \in [V]$. Therefore, the upper bound of subsequent uncertainty at the t -th scale is determined by the sum of conditional entropies of all tokens in R_t :

$$H(R_t | R_{<t}) \leq \sum_{i=1}^{N_t} H(r_{t,i} | R_{<t}). \quad (3)$$

Combining Equations 2 and 3, it follows that maintaining highest-entropy tokens ensures the upper bound of uncertainty remains controllable while maximizing potential information gain to reduce future uncertainty, thereby facilitating the autoregressive generation process. Meanwhile, pruning the lowest-entropy tokens has limited impact on potential information gain but effectively reduces attention computation cost, thus providing theoretical foundation for our entropy-guided token reduction method.

Scale-Level Generation Process Analysis. Existing methods (Guo et al., 2025a; Chen et al., 2025b; Li et al.,

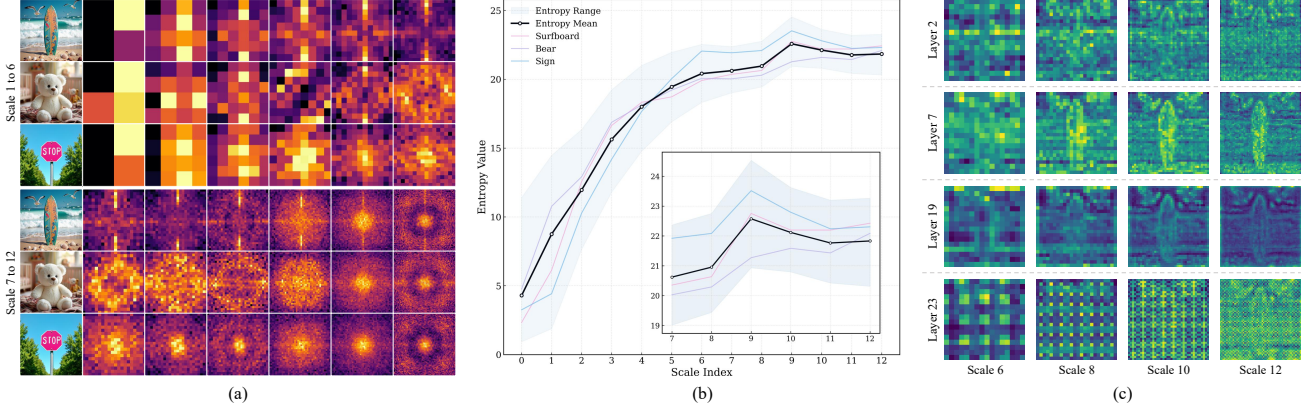


Figure 4. (a) Frequency spectrum of various instances at different scales during VAR generation. (b) Various entropy values across different scales during the inference process of Infinity-2B: We selected 600 prompts from GenEval and rewrote them. For each rewritten prompt, we generated four images using different random seeds. (c) Entropy heatmaps of token maps across different Transformer layers. Cross-layer spatial pattern variations: Shallow layers exhibit high-entropy regions resembling local noise or scattered dots, certain middle layers show high-entropy regions with clear subject contours, while deeper layers display regular periodic grid-like patterns in high-entropy regions. Cross-layer overall entropy variations: For example, token map at the 19-th layer has relatively low overall entropy.

2025d) employ frequency to heuristically partition the later stage and perform token reduction within it. As shown in Figure 4 (a), we analyze the frequency spectrum evolution of token maps at different scales during generation across the three instances. Although a general coarse-to-fine process and certain stage-specific characteristics are observable, the distribution, content, and diffusion evolution of frequency components vary significantly across instances, making it difficult to adaptively and accurately partition the later stage through frequency analysis. Furthermore, some instances exhibit high-frequency patterns even in the middle scales, indicating more opportunities for token reduction prior to the later stage. While these works are highly novel and interesting and have achieved impressive results, we realize that relying solely on frequency, the physical property of images, makes it difficult to precisely capture the modeling process. Only by addressing the limitations of heuristic stage partition, non-adaptive schedules, and limited acceleration scope from the intrinsic properties of VAR generation, its acceleration potential can be further unleashed.

We calculate the predictive entropy for all instances across scales. Figure 4 (b) illustrates the overall entropy range and mean, while highlighting the entropy variations for the three aforementioned instances: surfboard, bear, and sign. The subfigure reveals that the entropy of three instances fluctuates and diverges from one another at the larger scales, significantly deviating from the entropy mean. This suggests that even from an entropy perspective, it remains challenging to accurately and adaptively partition the later stage. Unlike previous works, this frees us from the focus on later stage partition. Nevertheless, the entropy range, the entropy mean, and the three instances all exhibit a consistent two-stage dynamic: entropy grows rapidly at early scales, followed by a phase of relatively slow growth or unstable

fluctuation. This aligns with previous findings (Li et al., 2025d; Chen et al., 2025a;c) that VAR models constructs concepts and objects at early scales. This motivates leveraging the entropy growth inflection point to adaptively activate acceleration, avoiding quality degradation from premature reduction and limited acceleration from delayed reduction.

Layer-Level Generation Process Analysis. We further analyze the entropy characteristics of token maps across different Transformer layers at the same scale. Figure 4 (c) reveals significant layer-level entropy heterogeneity. First, different layers exhibit various spatial distributions of high-entropy regions, indicating their distinct spatial modeling patterns. Second, the overall (average) entropy at the same scale also varies across layers. These variations suggest a uniform reduction ratio across all layers is suboptimal. Instead, token reduction at the same scale should be layer-adaptive, allocating more computation to high-entropy layers while reducing more tokens in low-entropy layers.

3.3. NOVA

Figure 5 illustrates the NOVA framework at both scale-level and layer-level, which consists of three key components: Adaptive Acceleration Activation, Dual-Linkage Acceleration and Residual Cache Reuse.

Adaptive Acceleration Activation. At the scale-level, NOVA first determines the acceleration activation scale by online identifying the inflection point of the entropy growth across scales. For the token map R_t at the t -th scale, the predictive entropy of the i -th token $r_{t,i} \in [V]$ is defined as:

$$\mathcal{H}_{t,i} = H(r_{t,i} | R_{<t}) = - \sum_{v \in [V]} p_{t,i}(v) \log p_{t,i}(v), \quad (4)$$

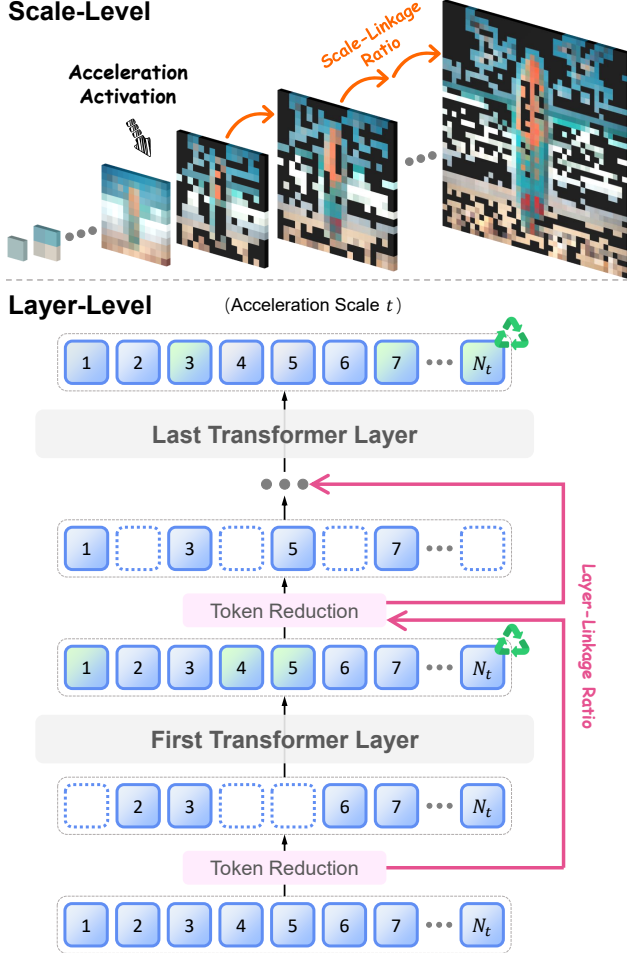


Figure 5. NOVA framework at both scale-level and layer-level.

where $p_{t,i}(\cdot)$ is the predicted class distribution for token $r_{t,i}$.

Since VAR performs parallel prediction for N_t tokens within the t -th scale, we adopt a factorized conditional likelihood within the token map R_t :

$$p(R_t | R_{<t}) = \prod_{i=1}^{N_t} p(r_{t,i} | R_{<t}). \quad (5)$$

Therefore, the joint predictive entropy of the token map R_t decomposes additively into token predictive entropy:

$$H(R_t | R_{<t}) = \sum_{i=1}^{N_t} H(r_{t,i} | R_{<t}) = \sum_{i=1}^{N_t} \mathcal{H}_{t,i}. \quad (6)$$

We aggregate the predictive entropies of all tokens in the token map R_t and calculate their mean to obtain the t -th scale overall predictive entropy $\bar{\mathcal{H}}_t$:

$$\bar{\mathcal{H}}_t \triangleq \frac{1}{N_t} H(R_t | R_{<t}) = \frac{1}{N_t} \sum_{i=1}^{N_t} \mathcal{H}_{t,i}. \quad (7)$$

In our earlier analysis, we found that the scale overall entropy $\bar{\mathcal{H}}_t$ exhibits a consistent two-stage dynamic as the scale increases. Therefore, using $\bar{\mathcal{H}}_t$ as a criterion, we online detect the decay of the entropy growth rate to identify the earliest scale where the growth rate decays and remains small as the acceleration activation scale. We define the discrete entropy growth rate g_t at scale t as:

$$g_t \triangleq \bar{\mathcal{H}}_t - \bar{\mathcal{H}}_{t-1}, \quad t = 2, \dots, T. \quad (8)$$

As a training-free acceleration framework, NOVA cannot access the overall entropy of all future scales at the beginning of inference. Therefore, we preserve the first t_{est} scales without token reduction to estimate the early entropy growth baseline for the current instance:

$$\eta \triangleq \frac{1}{t_{\text{est}} - 1} \sum_{t=2}^{t_{\text{est}}} g_t, \quad (9)$$

Considering the volatile fluctuations in $\bar{\mathcal{H}}_t$, we perform a moving average \tilde{g}_t on two adjacent discrete entropy growth rates g_t obtained after the early entropy growth baseline estimation to mitigate misjudgments caused by oscillations: $\tilde{g}_t = (g_t + g_{t-1})/2$, where $t \geq t_{\text{est}} + 1$.

We identify the earliest scale t^* when the smoothed growth rate drops below a fraction $\alpha \in (0, 1)$ of the early entropy growth baseline η :

$$t^* \triangleq \min \{t \mid t \geq t_{\text{est}} + 1, \tilde{g}_t \leq \alpha \eta\}. \quad (10)$$

The scale t^* is regarded as the inflection point of the scale overall entropy growth. Consequently, NOVA activates acceleration at the scale $t^* + 1$.

Dual-Linkage Acceleration. The core of dual-linkage acceleration lies in dynamically adjusting and determining the distinct token reduction ratio for each scale or layer based on entropy variations of token maps. We design scale-linkage and layer-linkage ratio functions to realize.

For scale-linkage ratio function, we first assign each scale a base reduction ratio that progressively increases as generation proceeds. We then refine this base ratio by entropy growth rate g_t : if uncertainty is still changing rapidly, we reduce fewer tokens; if it trends toward stability, we reduce more. Thus, the token reduction ratio at the t -th scale is:

$$\text{Ratio}_t = \sigma \left(\frac{t - (t^* + 1)}{\tau} \right) - \lambda \cdot \tanh(g_t), \quad (11)$$

where $\sigma(\cdot)$ is the sigmoid function, λ is a scaling factor.

For layer-linkage ratio function, We dynamically refine the scale reduction ratio by computing the relative deviation between the current layer's overall entropy and the mean overall entropy of all preceding layers and use this as the

Table 1. Quantitative comparisons of perceptual quality on the GenEval and DPG-Bench benchmarks.

Methods	#Speed↑	#Latency↓	#Param↓	GenEval↑				DPG-Bench↑		
				Two Obj.	Position	Color Attri.	Overall	Global	Relation	Overall
HART	1.00 ×	1.12s	0.7B	0.62	0.13	0.18	0.51	87.10	92.95	80.89
+FastVAR	1.30 ×	0.86s	0.7B	0.57	0.16	0.19	0.50	86.21	92.48	80.71
+SparseVAR	1.38 ×	0.81s	0.7B	0.60	0.12	0.21	0.50	86.63	92.54	80.70
+NOVA	1.62 ×	0.69s	0.7B	0.60	0.13	0.17	0.51	86.88	92.53	80.84
Infinity-2B	1.00 ×	2.43s	2.0B	0.85	0.45	0.54	0.73	85.10	92.37	83.12
+FastVAR	2.45 ×	0.99s	2.0B	0.81	0.37	0.52	0.70	84.41	92.76	82.86
+SparseVAR	1.66 ×	1.46s	2.0B	0.84	0.42	0.54	0.72	84.11	92.70	82.56
+SkipVAR	2.23 ×	1.09s	2.0B	0.84	0.39	0.60	0.72	84.19	93.07	82.94
+NOVA	2.89 ×	0.84s	2.0B	0.86	0.42	0.58	0.72	84.36	92.68	82.93
Infinity-8B	1.00 ×	1.51s	8.0B	0.94	0.58	0.68	0.80	85.10	94.50	86.60
+FastVAR	1.26 ×	0.79s	8.0B	0.92	0.55	0.68	0.78	84.80	92.30	86.46
+SparseVAR	1.22 ×	0.82s	8.0B	0.91	0.57	0.69	0.77	83.91	90.52	86.40
+NOVA	1.33 ×	0.75s	8.0B	0.92	0.58	0.69	0.79	84.27	93.61	86.53

criterion for adjusting the token reduction ratio at the current layer. For the t -th scale and j -th layer, the mean overall entropy $\mu_{t,j-1}$ of the preceding $j-1$ layers is:

$$\mu_{t,j-1} = \frac{1}{j-1} \sum_{k=1}^{j-1} \bar{\mathcal{H}}_{t,k}, \quad j \geq 2. \quad (12)$$

Therefore, $\Delta_{t,j} = (\bar{\mathcal{H}}_{t,j} - \mu_{t,j-1}) / \mu_{t,j-1}$ is the adjustment for the j -th layer's overall entropy $\bar{\mathcal{H}}_{t,j}$. The token reduction ratio $\text{Ratio}_{t,j}$ at the t -th scale and j -th layer is:

$$\text{Ratio}_{t,j} = \begin{cases} \text{Ratio}_t, & j = 1, \\ \text{Ratio}_t - \Delta_{t,j} \text{Ratio}_t, & j \geq 2. \end{cases} \quad (13)$$

Finally, pruning low-entropy tokens according to the token reduction ratio can achieve dual-linkage acceleration.

Residual Cache Reuse. As a dense prediction task, visual generation requires preserving a coherent two-dimensional structure, we employ residual cache reuse to compensate for pruned low-entropy tokens. At scales with $t \geq t^*$, the residual cache is activated and updated. The layer transformation at the j -th layer (Transformer layer j) for the t -th scale can be expressed as:

$$R_{t,j}^{\text{output}} = \text{Layer}_j \left(R_{t,j}^{\text{input}} \right), \quad (14)$$

Consequently, we construct a layer-wise residual cache:

$$\text{Cache}_{t,j} = R_{t,j}^{\text{output}} - R_{t,j}^{\text{input}}. \quad (15)$$

When predicting the next scale $t+1$ at j -th layer, for those pruned tokens, we interpolate $\text{Cache}_{t,j}$ into $\text{Cache}_{t \rightarrow t+1,j}$ and reconstruct the layer output by reusing residual cache:

$$R_{t,j}^{\text{output}} = \text{Cache}_{t \rightarrow t+1,j} + R_{t,j}^{\text{input}}. \quad (16)$$

By reusing dynamic residual information rather than static tokens, NOVA preserves fine-grained structural cues while avoiding redundant computation on low-entropy tokens.

4. Experiments

4.1. Experimental Settings

Models and Benchmarks. We employ text-to-image VAR models to evaluate NOVA, including Infinity-2B, Infinity-8B (Han et al., 2025), and HART-0.7B (Tang et al., 2024). All selected backbones are capable of high-resolution image generation at 1024×1024 . We utilize GenEval (Ghosh et al., 2023), DPG-Bench (Hu et al., 2024), and MJHQ-30K (Li et al., 2024a) to evaluate generation quality, which are widely adopted for assessing semantic alignment and the perceptual quality of generated images. Moreover, we use ImageReward (Xu et al., 2023) and HPSv2.1 (Wu et al., 2023b). To quantify efficiency, we report the average inference latency and the corresponding speedup ratio achieved by our method.

Implementation Details. To ensure a fair comparison, we evaluate NOVA against all open-source baselines using their default hyperparameter settings. And we configure our adaptive acceleration activation strategy with $t_{\text{est}} = 5$ and $\alpha = 0.5$, and set the dual-linkage function with $\tau = 0.8$ and $\lambda = 0.1$. All experiments are conducted on a single NVIDIA RTX 3090 GPU, except for Infinity-8B, which is evaluated on an NVIDIA H200 GPU due to its larger model size.

4.2. Main Results

Quantitative Performance Comparison. As shown in Table 1 and Table 3, we assess both generation quality and inference efficiency for 1024×1024 image generation on GenEval, DPG-Bench, and MJHQ-30K. Compared with other comparable models, NOVA consistently achieves a superior balance of efficiency and performance. Specifically, for Infinity-2B, NOVA delivers $2.89 \times$ speedup while pre-

Table 2. Quantitative evaluation on ImageReward and HPSv2.1, two widely used human preference benchmarks.

Methods	Latency	ImageReward			HPSv2.1				
		Score↑	CLIP-Score↑	Anime↑	Concept-Art↑	Paintings↑	Photo↑	Overall↑	
Infinity-2B	2.43s	0.921	0.27	31.63	30.26	30.28	29.27	30.36	
+FastVAR	0.99s	0.903	0.26	31.12	30.15	29.92	28.86	29.95	
+SkipVAR	1.09s	0.908	0.27	30.11	30.18	30.13	29.07	30.22	
+SparseVAR	1.46s	0.895	0.26	31.22	29.61	29.10	28.21	29.53	
+NOVA	0.84s	0.911	0.27	31.40	30.06	30.21	29.11	30.20	
Infinity-8B	1.51s	1.030	0.28	32.40	31.17	30.78	29.35	30.92	
+FastVAR	0.79s	1.028	0.28	31.80	30.42	29.89	29.87	30.24	
+SkipVAR	0.82s	1.032	0.27	32.01	30.58	30.46	29.09	30.44	
+NOVA	0.75s	1.035	0.28	32.03	30.71	30.25	29.15	30.54	

serving approximately original GenEval Overall score 0.72. Notably, NOVA attains the best performance on Two Object sub-metric, outperforming both the original Infinity-2B and other acceleration methods. Moreover, on DPG-Bench and MJHQ-30K, results also confirm that NOVA preserves high-fidelity visual quality under acceleration. Furthermore, on larger-size and other VAR models such as Infinity-8B and HART, NOVA consistently delivers substantial acceleration, demonstrating its broad applicability and generalizability across diverse model architectures and sizes.

Table 3. Performance on GenEval↑ benchmark.

Methods	Landscape		People		Food	
	FID↓	CLIP↑	FID↓	CLIP↑	FID↓	CLIP↑
HART	25.43	26.82	30.61	28.47	30.37	28.03
+FastVAR	22.52	26.51	28.19	28.34	30.97	28.25
+NOVA	22.81	26.56	28.09	28.33	30.74	28.40
Infinity-2B	29.29	26.18	28.15	27.97	30.73	26.70
+FastVAR	28.08	26.58	27.99	28.31	29.95	27.08
+NOVA	29.29	26.14	27.88	29.29	29.91	27.03

Quantitative Performance on Human Preference. We further evaluate the impact of NOVA’s acceleration on perceptual quality using human preference benchmarks with ImageReward and HPSv2.1. In Table 2, despite the aggressive reduction in token usage, NOVA maintains high alignment with human aesthetic preferences. Surprisingly, on ImageReward, NOVA obtains a score of 1.035 on Infinity-8B, outperforming the initial Infinity-8B (1.030). This breaks the conventional wisdom that accelerating through token pruning necessarily leads to performance loss. On HPSv2.1, NOVA remains comparable to the unpruned baseline, confirming that the generated images are free of perceptible artifacts and maintain high artistic quality.

Visual Comparison. In Figure 7 and Figure 6, we provide visual comparisons to illustrate the performance of NOVA across different backbones and against comparable token reduction acceleration methods. These results indicate that

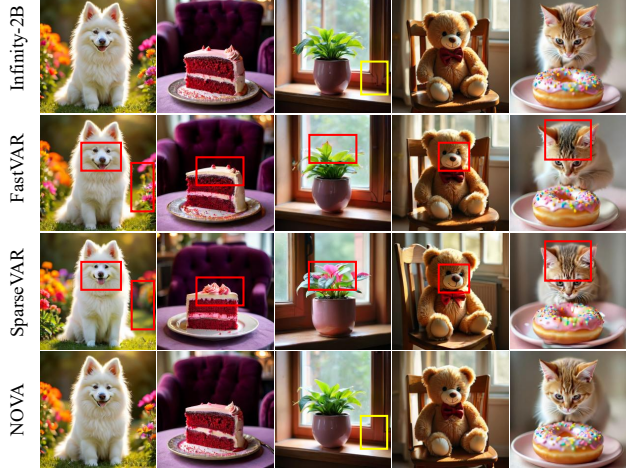


Figure 6. Visual comparison between NOVA and other training-free comparable methods on Infinity-2B. Red and yellow boxes highlight the finer details in visualization.

under the adaptive acceleration activation and dual-linkage acceleration, NOVA achieves near-lossless visual quality mitigates semantic loss, structural distortion, and detail collapse. Notably, in the yellow-box region, NOVA generates clearer and more logically consistent structural details than the original Infinity-2B, aligning better with human preference.

Table 4. Ablation of token selection metrics on Infinity-2B.

Methods	GenEval ↑			
	Two Obj.	Position	Color Attri.	Overall
Infinity-2B	0.85	0.45	0.54	0.73
+NOVA w/ Attn	0.84	0.38	0.52	0.69
+NOVA w/ MSE	0.82	0.42	0.52	0.71
+NOVA w/ Entropy	0.86	0.42	0.54	0.72

4.3. Ablation and Analysis

Effectiveness of Entropy Analysis. To examine the effectiveness of our entropy-based method for token reduction,



Figure 7. Visual comparisons between NOVA and backbones, including Infinity-2B, Infinity-8B, and HART-0.7B.

we conduct an ablation study comparing it with Attention-based (Attn) and MSE-based (MSE) alternatives on Infinity-2B. All variants adopt the same dual-linkage configuration for fair comparison. As shown in Table 4, the MSE-based method leads to a noticeable drop in overall GenEval performance, while the entropy-based variant achieves the best overall score among all compared methods. Similar to SparseVAR (Chen et al., 2025b), we treat MSE metric as a proxy for frequency signal magnitude. These results suggest that frequency signals alone may not reliably reflect their impact on potential information, whereas entropy provides a more informative criterion for identifying tokens that contribute important information in the pruning process.

Table 5. Ablation on effectiveness of dual-linkage acceleration on Infinity-2B. \dagger denotes the variants’ scale-level reduction ratios are fixed following FastVAR, \ddagger denotes the variants’ scale-level reduction ratios following SparseVAR.

Methods	Scale-Linkage	Layer-Linkage	Speedup	GenEval \uparrow
NOVA \dagger	\times	\times	2.55 \times	0.69
NOVA \dagger	\times	\checkmark	2.34 \times	0.70
NOVA \ddagger	\times	\times	2.15 \times	0.71
NOVA \ddagger	\times	\checkmark	2.22 \times	0.71
NOVA	\checkmark	\times	2.85 \times	0.71
NOVA	\checkmark	\checkmark	2.89 \times	0.72

Effectiveness of Dual-Linkage Acceleration. We conduct an ablation study covering two no-linkage and three single-linkage variants for examine the effectiveness of dual-linkage acceleration. All variants employ adaptive acceleration activation to ensure a fair comparison. As shown in Table 5, both no-linkage variants suffer from an inherent efficiency-quality trade-off. Further, enabling either scale-linkage or layer-linkage alone consistently improves over the corresponding no-linkage variants, while jointly applying dual-linkage pushes this improvement to the best overall efficiency and performance trade-off.

Statistical Analysis of Acceleration Activation Scale. We statistically analyze the acceleration activation scale on MJHQ-30K by examining its distribution across image categories. In Figure 8, diverse image categories exhibit distinct activation distributions, indicating that pruning on

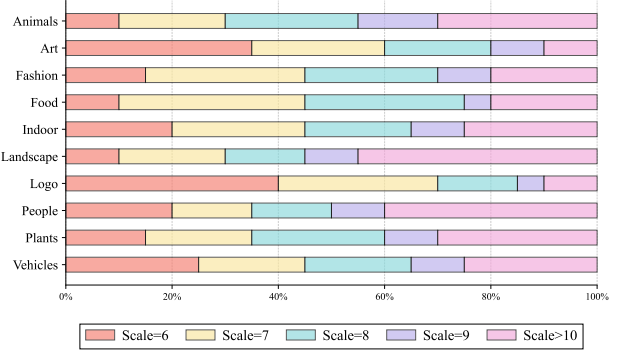


Figure 8. Distribution of acceleration activation scale ratios of NOVA across different categories of the MJHQ-30K benchmark.

set depends on content: fine-grained textures necessitate later pruning, whereas simple global structures allow earlier activation. The results suggest that NOVA can effectively capture context-specific generation characteristics and adaptively identify appropriate acceleration scales, rather than relying on fixed or heuristic reduction schedules.

5. Conclusion

This paper introduces NOVA, a training-free acceleration framework for VAR models. By utilizing dual-linkage entropy analysis, NOVA adaptively online identifies the acceleration activation scale through entropy growth inflection point detection. NOVA also dynamically computes distinct token reduction ratios across both scales and layers, pruning low-entropy tokens and reusing residual cache to accelerate inference and maintain quality. Extensive experiments validate NOVA as a simple yet effective acceleration method.

Impact Statement

This paper presents work whose goal is to advance the field of Machine Learning. There are many potential societal consequences of our work, none of which we feel must be specifically highlighted here.

References

Ben-Hamu, H., Gat, I., Severo, D., Nolte, N., and Kar rer, B. Accelerated sampling from masked diffusion models via entropy bounded unmasking. *arXiv preprint arXiv:2505.24857*, 2025.

Cao, H., Tan, C., Gao, Z., Xu, Y., Chen, G., Heng, P.-A., and Li, S. Z. A survey on generative diffusion models. *IEEE transactions on knowledge and data engineering*, 36(7):2814–2830, 2024.

Chen, Z., Chu, R., Chen, Y., Zhang, S., Wei, Y., Zhang, Y., and Liu, X. Tts-var: A test-time scaling framework for visual auto-regressive generation. *arXiv preprint arXiv:2507.18537*, 2025a.

Chen, Z., Fan, J., Yu, Z., Zhuang, B., and Tan, M. Frequency-aware autoregressive modeling for efficient high-resolution image synthesis. In *Proceedings of the IEEE/CVF International Conference on Computer Vision*, pp. 17140–17149, 2025b.

Chen, Z., Ma, X., Fang, G., and Wang, X. Collaborative decoding makes visual auto-regressive modeling efficient. In *Proceedings of the Computer Vision and Pattern Recognition Conference*, pp. 23334–23344, 2025c.

Croitoru, F.-A., Hondu, V., Ionescu, R. T., and Shah, M. Diffusion models in vision: A survey. *IEEE transactions on pattern analysis and machine intelligence*, 45(9):10850–10869, 2023.

Dubey, A., Gupta, O., Raskar, R., Rahwan, I., and Naik, N. Regularizing prediction entropy enhances deep learning with limited data. In *Proceedings of the Neural Information Processing Systems (NIPS)*, 2017.

Ghosh, D., Hajishirzi, H., and Schmidt, L. Geneval: An object-focused framework for evaluating text-to-image alignment. *Advances in Neural Information Processing Systems*, 36:52132–52152, 2023.

Guo, H., Li, Y., Zhang, T., Wang, J., Dai, T., Xia, S.-T., and Benini, L. Fastvar: Linear visual autoregressive modeling via cached token pruning. *arXiv preprint arXiv:2503.23367*, 2025a.

Guo, L., Xue, Z., Xu, Z., and Xu, H. Demospeedup: Accelerating visuomotor policies via entropy-guided demonstration acceleration. *arXiv preprint arXiv:2506.05064*, 2025b.

Han, J., Liu, J., Jiang, Y., Yan, B., Zhang, Y., Yuan, Z., Peng, B., and Liu, X. Infinity: Scaling bitwise autoregressive modeling for high-resolution image synthesis. In *Proceedings of the Computer Vision and Pattern Recognition Conference*, pp. 15733–15744, 2025.

He, Y., He, Y., He, S., Chen, F., Zhou, H., Zhang, K., and Zhuang, B. Neighboring autoregressive modeling for efficient visual generation. *arXiv preprint arXiv:2503.10696*, 2025.

Hu, X., Wang, R., Fang, Y., Fu, B., Cheng, P., and Yu, G. Ella: Equip diffusion models with llm for enhanced semantic alignment. *arXiv preprint arXiv:2403.05135*, 2024.

Huang, Y., Chen, W., Zheng, W., Duan, Y., Zhou, J., and Lu, J. Spectralar: Spectral autoregressive visual generation. *arXiv preprint arXiv:2506.10962*, 2025.

Jiao, S., Zhang, G., Qian, Y., Huang, J., Zhao, Y., Shi, H., Ma, L., Wei, Y., and Jie, Z. Flexvar: Flexible visual autoregressive modeling without residual prediction. *arXiv preprint arXiv:2502.20313*, 2025.

Kumar, A., Nair, N. G., and Patel, V. M. Scale-wise var is secretly discrete diffusion. *arXiv preprint arXiv:2509.22636*, 2025.

Kumbong, H., Liu, X., Lin, T.-Y., Liu, M.-Y., Liu, X., Liu, Z., Fu, D. Y., Re, C., and Romero, D. W. Hmar: Efficient hierarchical masked auto-regressive image generation. In *Proceedings of the Computer Vision and Pattern Recognition Conference*, pp. 2535–2544, 2025.

Li, C., Zhang, J., Liu, S., Lin, S., Shi, Z., Li, Z., and Chang, X. Efficient training for human video generation with entropy-guided prioritized progressive learning. *arXiv preprint arXiv:2511.21136*, 2025a.

Li, D., Kamko, A., Akhgari, E., Sabet, A., Xu, L., and Doshi, S. Playground v2. 5: Three insights towards enhancing aesthetic quality in text-to-image generation. *arXiv preprint arXiv:2402.17245*, 2024a.

Li, J., Ma, Y., Zhang, X., Wei, Q., Liu, S., and Zhang, L. Skipvar: Accelerating visual autoregressive modeling via adaptive frequency-aware skipping. *arXiv preprint arXiv:2506.08908*, 2025b.

Li, K., Chen, Z., Yang, C.-Y., and Hwang, J.-N. Memory-efficient visual autoregressive modeling with scale-aware kv cache compression. *arXiv preprint arXiv:2505.19602*, 2025c.

Li, S., Wang, K., Khan, S., Khan, F. S., Yang, J., and Wang, Y. Stagevar: Stage-aware acceleration for visual autoregressive models. *arXiv preprint arXiv:2512.16483*, 2025d.

Li, X., Qiu, K., Chen, H., Kuen, J., Lin, Z., Singh, R., and Raj, B. Controlvar: Exploring controllable visual autoregressive modeling. *arXiv preprint arXiv:2406.09750*, 2024b.

Li, Y., Wang, H., et al. Freqexit: Enabling early-exit inference for visual autoregressive models via frequency-aware guidance. In *The Thirty-ninth Annual Conference on Neural Information Processing Systems*.

Ma, X., Zhou, M., Liang, T., Bai, Y., Zhao, T., Li, B., Chen, H., and Jin, Y. Star: Scale-wise text-conditioned autoregressive image generation. *arXiv preprint arXiv:2406.10797*, 2024.

Meni, M. J., White, R. T., Mayo, M. L., and Pilkiewicz, K. R. Entropy-based guidance of deep neural networks for accelerated convergence and improved performance. *Information Sciences*, 681:121239, 2024.

Peer, D., Keulen, B., Stabinger, S., Piater, J., and Rodríguez-Sánchez, A. Improving the trainability of deep neural networks through layerwise batch-entropy regularization. *arXiv preprint arXiv:2208.01134*, 2022.

Qin, Z., Lv, Y., Lin, M., Guo, H., Zhang, Z., Zou, D., and Lin, W. Head-aware kv cache compression for efficient visual autoregressive modeling. *arXiv preprint arXiv:2504.09261*, 2025.

Qu, Y., Yuan, K., Hao, J., Zhao, K., Xie, Q., Sun, M., and Zhou, C. Visual autoregressive modeling for image super-resolution. *arXiv preprint arXiv:2501.18993*, 2025.

Rajagopalan, S., Narayan, K., and Patel, V. M. Restorer: Visual autoregressive generation for all-in-one image restoration. *arXiv preprint arXiv:2505.18047*, 2025.

Ren, S., Yu, Y., Ruiz, N., Wang, F., Yuille, A., and Xie, C. M-var: Decoupled scale-wise autoregressive modeling for high-quality image generation. *arXiv preprint arXiv:2411.10433*, 2024.

Shen, H., Zhang, J., Xiong, B., Hu, R., Chen, S., Wan, Z., Wang, X., Zhang, Y., Gong, Z., Bao, G., et al. Efficient diffusion models: A survey. *arXiv preprint arXiv:2502.06805*, 2025.

Tang, H., Wu, Y., Yang, S., Xie, E., Chen, J., Chen, J., Zhang, Z., Cai, H., Lu, Y., and Han, S. Hart: Efficient visual generation with hybrid autoregressive transformer. *arXiv preprint arXiv:2410.10812*, 2024.

Tian, K., Jiang, Y., Yuan, Z., Peng, B., and Wang, L. Visual autoregressive modeling: Scalable image generation via next-scale prediction. *Advances in neural information processing systems*, 37:84839–84865, 2024.

Vincenti, J., Jazbec, M., and Xia, G. Dynamic mixture-of-experts for visual autoregressive model. *arXiv preprint arXiv:2510.08629*, 2025.

Wang, R., Zhou, Q., and Zheng, G. Edrl: Entropy-guided disentangled representation learning for unsupervised domain adaptation in semantic segmentation. *Computer methods and programs in biomedicine*, 240:107729, 2023.

Wang, Y., Guo, L., Li, Z., Huang, J., Wang, P., Wen, B., and Wang, J. Training-free text-guided image editing with visual autoregressive model. *arXiv preprint arXiv:2503.23897*, 2025.

Wu, H., Fan, X., Wu, Z., and Cao, L. Nested autoregressive models, 2025. URL <https://arxiv.org/abs/2510.23028>.

Wu, J., Chen, X., Shi, B., Li, S., and Xu, K. Sega: Structural entropy guided anchor view for graph contrastive learning. In *International Conference on Machine Learning*, pp. 37293–37312. PMLR, 2023a.

Wu, X., Hao, Y., Sun, K., Chen, Y., Zhu, F., Zhao, R., and Li, H. Human preference score v2: A solid benchmark for evaluating human preferences of text-to-image synthesis. *arXiv preprint arXiv:2306.09341*, 2023b.

Xiao, Y., Shu, K., Zhang, H., Yin, B., Cheang, W. S., Wang, H., and Gao, J. Eggesture: Entropy-guided vector quantized variational autoencoder for co-speech gesture generation. In *Proceedings of the 32nd ACM International Conference on Multimedia*, pp. 6113–6122, 2024.

Xie, R., Zhao, T., Yuan, Z., Wan, R., Gao, W., Zhu, Z., Ning, X., and Wang, Y. Litevar: Compressing visual autoregressive modelling with efficient attention and quantization. *arXiv preprint arXiv:2411.17178*, 2024.

Xu, J., Liu, X., Wu, Y., Tong, Y., Li, Q., Ding, M., Tang, J., and Dong, Y. Imagereward: Learning and evaluating human preferences for text-to-image generation. *Advances in Neural Information Processing Systems*, 36:15903–15935, 2023.

Yang, Y., Wu, Q., He, B., Peng, H., Yang, R., Hao, Z., and Liao, Y. Sebot: Structural entropy guided multi-view contrastive learning for social bot detection. In *Proceedings of the 30th ACM SIGKDD conference on knowledge discovery and data mining*, pp. 3841–3852, 2024.

Yang, Z., Zhang, G., Wu, J., Yang, J., Sheng, Q. Z., Peng, H., Li, A., Xue, S., and Su, J. Minimum entropy principle guided graph neural networks. In *Proceedings of the sixteenth ACM international conference on web search and data mining*, pp. 114–122, 2023.

Zhang, K., Yang, R., Zhang, Y., You, S., and Huang, T. Actvar: Activating mixtures of weights and tokens for efficient visual autoregressive generation. *arXiv preprint arXiv:2511.12893*, 2025a.

Zhang, Q., Dai, X., Yang, N., An, X., Feng, Z., and Ren, X. Var-clip: Text-to-image generator with visual autoregressive modeling. *arXiv preprint arXiv:2408.01181*, 2024.

Zhang, Y., Liu, J., Shi, Y., Zhang, Q., Miao, D., Wang, C., and Cao, L. Markovian scale prediction: A new era of visual autoregressive generation. *arXiv preprint arXiv:2511.23334*, 2025b.